

THIRTEENTH EUROPEAN ROTORCRAFT FORUM

26
paper no. 80

COMPUTATION OF TRANSONIC POTENTIAL FLOW
ON HELICOPTER ROTOR BLADES

M. Costes

ONERA, b.p. 72, 92322 Chatillon cedex, France

and

H.E. Jones

U.S. Army Aeroflightdynamics Directorate, AVSCOM,
Ames Research Center, Moffett Field, CA 94035-1099, USA

September 8-11, 1987

ARLES, FRANCE

Association Aeronautique et Astronautique de France (A.A.A.F.)

Abstract

Two computer codes , the Full-Potential 3D (FP3D) code and the Full-Potential Rotor (FPR) code have recently been developed. Both of these codes solve the three-dimensional conservative formulation of the full potential equation. The FPR code was developed at the US Army Aeroflightdynamics Directorate (AFDD) while the FP3D code was a joint development by ONERA and AFDD. Both of these codes were used to predict the nonlifting, unsteady flow over a rotor operating at high advance ratio and tip speed. Three different rotor tip planform shapes were studied: a rectangular tip, a 30 ° aft swept tip and a 30 ° forward swept tip. Results of these computations are compared to results obtained using an earlier small-disturbances code. Also, the lifting flow over a rectangular tip operating at a slightly different condition was computed. These results are also compared with the small disturbances computations and with experimental results.

1 Introduction

The flow appearing on helicopter rotor blades involves many very complex phenomena such as transonic flows on the advancing side of the rotor disk and stall on the retreating one. These different phenomena cannot be computed accurately by the same method in a reasonably short time as needed for design purposes. This is the reason why more specialised methods are used to take into account one particular regime.

Transonic flow conditions impose major limitations on high speed flight. These limitations manifest themselves in high vibration levels, power divergence, noise and component fatigue. Recent efforts to study this problem have centered on the use of finite-difference methods to compute the complex flow field near the tip of the rotor [1-4]. The goal of these studies has been to develop methods which will allow for the rapid and accurate prediction of rotor loads for use in the design and analysis process. Potential methods have been chosen by many researchers because they offer the best compromise between simple linear methods currently used by industry [5] and full Navier-Stokes methods.

The first approach to use a potential method to study the effect of rotor planform was made at ONERA, in particular by Desopper [6], using a small disturbances formulation of the potential equation . Strawn of the US Army Aeroflightdynamics Directorate (AFDD) has developed a full potential model called FPR. This code has been used to study blade-vortex interactions and to investigate coupling between finite-difference methods and integral methods. A new finite difference code solving the full potential equation has been developed recently through a joint effort between ONERA and AFDD (FP3D code). It uses an algorithm very similar to that of the FPR code and neither of them has been exercised to study blade planform effects until the present paper.

In a first part of this paper the equations solved by the three codes will be

presented; the solution procedure will also be briefly developed, showing in particular the similarities and differences between the FP3D and the FPR code. Then three dimensional computations simulating the flow appearing on a rotor blade for the advancing side will be presented for various blade tip shapes. The computations are similar to those already presented by Desopper.

2 Presentation of the finite difference codes

2.1 Introduction

It is generally considered that the transonic flow present on the advancing side of helicopter rotor blades is low enough so that the flow might be assumed as isentropic and irrotational (local Mach number smaller than 1.3). Under this approximation, the flow behaviour is described by the potential equation which consists of the set of the mass conservation equation and the Bernoulli equation. In a non dimensional form, where the velocities are normalized by the freestream value, distances by a reference chord c , time by the term $(c/a\infty)$ and density by its freestream value, the mass conservation equation and the Bernoulli equation take the form:

$$(1) \quad \rho_t + (\rho\phi_x)_x + (\rho\phi_y)_y + (\rho\phi_z)_z = 0$$

$$(2) \quad \rho = \left[1 + \frac{\gamma-1}{2} (M_\infty^2 - 2\phi_t^2 - \phi_x^2 - \phi_y^2 - \phi_z^2) \right]^{1/(\gamma-1)}$$

With no other approximations, substituting (2) into (1) gives the full potential equation in a non conservative form, while a small disturbances hypothesis can be done to get a simpler form of the equation where non linear transonic terms still remain.

2.2 Presentation of the small disturbances code

The small disturbances code was developed jointly by ONERA and the AFDD at Ames within the framework of a M.O.U. [7]. The equation was essentially valid for azimuthes close to $\psi = 90^\circ$. It has been extended to a larger azimuthal sector by Desopper [6] by writing the equation in the local frame linked to the velocity vector. The equation solved is the following :

$$(3) \quad M_{\omega R}^2 \epsilon^2 \phi_{tt} + 2M_{\omega R}^2 \frac{\epsilon}{\delta^{2/3}} u_1 \phi_{xt} - 2M_{\omega R}^2 \frac{\epsilon^2}{\delta^{2/3}} u_2 \phi_{yt} =$$

$$\frac{1}{(u_1^2 + u_2^2)} (u_1^2 \phi_{xx} + u_2^2 \epsilon^2 \phi_{yy} - 2u_1 u_2 \epsilon \phi_{xy}) \times$$

$$\left(\frac{1 - M_{\omega R}^2 (u_1^2 + u_2^2)}{\delta^{2/3}} - M_{\omega R}^2 (\gamma+1) (u_1 \phi_x - \epsilon u_2 \phi_y) \right)$$

$$\begin{aligned}
& + \frac{u_2^2}{(u_1^2 + u_2^2)} \frac{\phi_{xx}}{\delta^{2/3}} + \frac{u_1^2}{(u_1^2 + u_2^2)} \frac{\epsilon^2}{\delta^{2/3}} \phi_{yy} + \frac{2u_1 u_2}{(u_1^2 + u_2^2)} \frac{\epsilon^2}{\delta^{2/3}} \phi_{xy} \\
& + \phi_{zz} + \frac{\epsilon}{\delta^{2/3}} M_{\omega R}^2 (\mu \sin t + u_2) \phi_x + \frac{\epsilon^2}{\delta^{2/3}} M_{\omega R}^2 (u_1 + \mu \cos t) \phi_y
\end{aligned}$$

with

$$\begin{cases} u_1 = y + \mu \cos t \\ u_2 = \epsilon x + \mu \sin t \end{cases}$$

The transonic term (first term on the right hand side) and the ϕ_{yt} term are treated in a simplified way; in the reduced coordinates system linked to the blade (ξ, η, ζ) , only the derivatives in the ξ direction are actually computed. The spatial differentiation uses a modified Murman and Cole scheme to maintain stability in the supersonic regions. The boundary conditions are a tangency condition on the blade surface, Dirichlet conditions upstream and at the grid tip, Neumann conditions elsewhere. A term representing the spanwise gradient influence on the boundary conditions has been added to improve the blade representation for swept or anhedral tips. The initial condition is given by a steady computation at the azimuth $\psi = 0^\circ$. The equation is solved using an A.D.I. method.

A complete description of the code and many computed results can be found in references [6,8,9]. The method has been widely used for several years for blade tip design, acoustic studies and aeroelastic analysis [10,11].

2.3 Presentation of the full potential codes

The two full potential codes used for the computations presented in this paper have the same general formulation which was developed by Caradonna and Steger [12]. The equations (1,2) are valid in a Galilean frame (X, Y, Z, T) which was chosen in both codes to be linked to the air at freestream conditions. A coordinates transformation is made to get surface coordinates which map the body surface:

$$(4) \quad \begin{cases} \xi = \xi(X, Y, Z, T) \\ \eta = \eta(X, Y, Z, T) \\ \zeta = \zeta(X, Y, Z, T) \\ \tau = T \end{cases}$$

Conservation form to the equation (1) can be maintained with this coordinates transformation and the set of equations becomes:

$$(5) \quad (\rho/J)_\tau + (\rho U/J)_\xi + (\rho V/J)_\eta + (\rho W/J)_\zeta = 0$$

$$(6) \quad \rho = \left\{ 1 + \frac{\gamma-1}{2} \left[-2\phi_\tau - (U + \xi_T)\phi_\xi - (V + \eta_T)\phi_\eta - (W + \zeta_T)\phi_\zeta \right] \right\}^{1/\gamma-1}$$

In these equations U, V and W are the contravariants velocities along the ξ , η and ζ directions and J is the Jacobian of the coordinates transformation. U, V and W are given by the expressions :

$$(7) \quad \begin{cases} U = \xi_T + A_1 \phi_\xi + A_4 \phi_\eta + A_5 \phi_\zeta \\ V = \eta_T + A_4 \phi_\xi + A_2 \phi_\eta + A_6 \phi_\zeta \\ W = \zeta_T + A_5 \phi_\xi + A_6 \phi_\eta + A_3 \phi_\zeta \end{cases}$$

A_1, A_2, A_3, A_4, A_5 and A_6 are metric terms which are given by the following expressions:

$$(8) \quad \begin{cases} A_1 = \nabla \xi \cdot \nabla \xi \\ A_2 = \nabla \eta \cdot \nabla \eta \\ A_3 = \nabla \zeta \cdot \nabla \zeta \end{cases} \quad \begin{cases} A_4 = \nabla \xi \cdot \nabla \eta \\ A_5 = \nabla \xi \cdot \nabla \zeta \\ A_6 = \nabla \eta \cdot \nabla \zeta \end{cases}$$

The temporal differentiation of equation (5) is obtained at first order by using an Euler backward differencing. The density is then eliminated by a Taylor expansion at first order, which gives:

$$\frac{\rho^{n+1}}{J} - \frac{\rho^n}{J} = \left[\frac{\rho^n}{J} + \left(\frac{1}{J} \frac{\partial \rho}{\partial \phi} \right)^n (\phi^{n+1} - \phi^n) \right] - \left[\frac{\rho^{n-1}}{J} + \left(\frac{1}{J} \frac{\partial \rho}{\partial \phi} \right)^{n-1} (\phi^n - \phi^{n-1}) \right]$$

The density derivative versus the velocity potential is obtained by differencing the Bernoulli equation (6), and one gets:

$$\frac{\partial \rho}{\partial \phi} = -\rho^{2-\gamma} [\partial_\tau + U \partial_\xi + V \partial_\eta + W \partial_\zeta]$$

This formulation gives then a conservative form for the full potential equation which takes the following form:

$$(9) \quad \begin{aligned} & (\rho/J)^n - (\rho/J)^{n-1} \\ & - \left(\rho^{2-\gamma}/J \right)^n \left[\partial_\tau + U \partial_\xi + V \partial_\eta + W \partial_\zeta \right]^n (\phi^{n+1} - \phi^n) \\ & + \left(\rho^{2-\gamma}/J \right)^{n-1} \left[\partial_\tau + U \partial_\xi + V \partial_\eta + W \partial_\zeta \right]^{n-1} (\phi^n - \phi^{n-1}) \\ & + h^{n+1} \left\{ \partial_\xi \left(\rho U/J \right)^{n+1} + \partial_\eta \left(\rho V/J \right)^{n+1} + \partial_\zeta \left(\rho W/J \right)^{n+1} \right\} = 0 \end{aligned}$$

where h^{n+1} is the time step at time level $n+1$.

Both codes use an approximate factorization technique for the system

inversion; an upstream density biasing is used to maintain stability for supercritical flows; a flow tangency condition on the rotor surface is implemented by setting the normal contravariant velocity W equal to zero; along the inner boundary plane normal to the rotor, the contravariant velocity V is set equal to η_t ; at the outer grid boundary, a nonreflection boundary condition similar to that used in [13] is implemented; for lifting cases, the shed vorticity, aligned with a coordinate plane from the trailing edge, is specified as a jump in potential Γ which is classically transported across the wake.

The two following sections show the differences in formulation between the two full potential codes to develop from (9) the actual equation solved: the FPR code solves (9) in a fully implicit way while the FP3D code has an explicit formulation in the spanwise direction; another important difference between the two codes is that the FP3D code has a consistent metrics differencing instead of a free stream subtraction method which corrects numerical errors due to incomplete metric cancellation.

2.3.1 Presentation of the FPR code

The FPR code was developed by Strawn [14,15,16] from a first code written by Bridgeman, Caradonna and Steger [17] for a fixed wing. In the equation (9) the fluxes are expanded in a delta form to express them at the n^{th} time step; this gives:

$$\begin{aligned}\partial_{\xi}(\rho U/J)^{n+1} &= \partial_{\xi}(\rho U/J)^n + \partial_{\xi}(\rho A_1/J)^n \partial_{\xi}(\phi^{n+1} - \phi^n) \\ \partial_{\eta}(\rho V/J)^{n+1} &= \partial_{\eta}(\rho V/J)^n + \partial_{\eta}(\rho A_2/J)^n \partial_{\eta}(\phi^{n+1} - \phi^n) \\ \partial_{\zeta}(\rho W/J)^{n+1} &= \partial_{\zeta}(\rho W/J)^n + \partial_{\zeta}(\rho A_3/J)^n \partial_{\zeta}(\phi^{n+1} - \phi^n)\end{aligned}$$

Finally, by reporting all the known terms on the right hand side of the equation, the system solved is the following one:

$$\begin{aligned}(10) \quad & \left\{ I + h^n (U^n \partial_{\xi} + V^n \partial_{\eta} + W^n \partial_{\zeta}) - h^n h^{n+1} / \beta^n \right. \\ & \left. [\partial_{\xi}(\rho A_1/J)^n \partial_{\xi} + \partial_{\eta}(\rho A_2/J)^n \partial_{\eta} + \partial_{\zeta}(\rho A_3/J)^n \partial_{\zeta}] \right\} (\phi^{n+1} - \phi^n) = \\ & (\phi^n - \phi^{n-1}) + (\beta^{n-1} / \beta^n) (h^n / h^{n-1}) (\phi^n - 2\phi^{n-1} + \phi^{n-2}) + h^n / \beta^n (\rho^n / J - \rho^{n-1} / J) \\ & + h^n \beta^{n-1} / \beta^n (U^{n-1} \partial_{\xi} + V^{n-1} \partial_{\eta} + W^{n-1} \partial_{\zeta}) (\phi^n - \phi^{n-1}) \\ & + h^n h^{n+1} / \beta^n [\partial_{\xi}(\rho U/J)^n + \partial_{\eta}(\rho V/J)^n + \partial_{\zeta}(\rho W/J)^n]\end{aligned}$$

where

$$\beta = \rho^{2-\gamma} / J$$

An approximate factorization technique resulting in the successive inversion of three one-dimensional problems in the ξ, η and ζ directions is then made. The density and the metrics are computed at each grid point and their values at mid cell necessary for the fluxes computation are obtained by a simple averaging; this implies a numerical error which results in a mass production, especially in the regions of poor grid resolution. This problem is solved using a free stream subtraction technique to give a correction term due to an incomplete metric cancellation; this term, which must be subtracted from the right hand side of the equation, is obtained by setting the potential to its freestream value.

2.3.2 Presentation of the FP3D code

The FP3D code is an extension and a generalization of a two dimensional code developed by Jones to study blade-vortex interaction [18,19]. As for the FPR code the fluxes are expanded in delta form to express them at the previous time step. However, all the terms of the equation in the spanwise direction are expressed explicitly, i.e. all are expressed at the previous time step and reported to the right hand side of the equation. The resulting equation is then:

$$(11) \left\{ I + h^n (U^n \partial_\xi + W^n \partial_\zeta) - h^n h^{n+1} / \beta^n [\partial_\xi (\rho A_1 / J)^n \partial_\xi + \partial_\zeta (\rho A_3 / J)^n \partial_\zeta] \right\} \\ (\phi^{n+1} - \phi^n) = \\ (\phi^n - \phi^{n-1}) + (\beta^{n-1} / \beta^n) (h^n / h^{n-1}) (\phi^n - 2\phi^{n-1} + \phi^{n-2}) + h^n / \beta^n (\rho^n / J - \rho^{n-1} / J) \\ + h^n \beta^{n-1} / \beta^n (U^{n-1} \partial_\xi + W^{n-1} \partial_\zeta) (\phi^n - \phi^{n-1}) \\ + h^n h^{n+1} / \beta^n [\partial_\xi (\rho U / J)^n + \partial_\zeta (\rho W / J)^n] \\ - h^n V^n \partial_\eta (\phi^n - \phi^{n-1}) + h^n \beta^{n-1} / \beta^n V^{n-1} \partial_\eta (\phi^{n-1} - \phi^{n-2}) + h^n h^{n+1} / \beta^n \partial_\eta (\rho V / J)^n$$

The explicit spanwise terms are on the last line of the equation; when they are equal to zero, the equation is similar to a two dimensional equation. This gives the possibility to write a code which is able to solve both 2D and 3D problems; in counterpart, the explicit spanwise formulation induces a CFL condition limiting the time step in relation to the minimum spanwise grid distance between two successive grid plans.

The FP3D equation is also approximately factored into two one-dimensional problems in the ξ and ζ directions. The metrics and the density are computed at each grid point and also at mid cell in each direction to compute the fluxes accurately.

3 Computational results

3.1 Computation parameters

The FPR code uses an O grid topology created by a p.d.e. grid generator code called GRAPE (figure 1); the O grid topology results in a very efficient use of grid points. The computation presented in the paper are made on a $81 \times 25 \times 20$ grid in the ξ, η and ζ directions respectively. The outer radius for each cylindrical O grid is located 4 chords from the rotor surface. Computational results show little sensitivity to outer boundary locations as close as 4 chords from the rotor surface (for nonlifting, 3-D computations). Typical spanwise grid distributions have inner boundaries located 3.5 chords from the rotor tip. The outer spanwise grid boundary is located approximately 2 chords beyond the tip of the rotor blade. For the low aspect ratio blades computed in this paper, the location of the outer spanwise grid boundary is limited by stability problems resulting from freestream supersonic grid velocities. The present density biasing scheme is unable to stabilize the calculation in regions where supersonic flow off the rotor tip is caused only by the motion of the grid. In addition, the grid off the blade surface is swept aft approximately along a characteristic line in order to better resolve the shock structure off the blade.

The FP3D code was written to use an H-grid topology like the code it was issued from [18,19] (figure 2). The present grid generator used is an algebraic grid generator code designed by Bredif at ONERA to compute potential flows using a finite element formulation [20]. The grid used for the computations shown below has $70 \times 18 \times 24$ points in the ξ, η and ζ directions. The grid resolution is a little poor in the spanwise direction but it has been chosen as a good compromise for first computations. The outer limits of the grid go up to 4 chords from the blade along each direction. In the spanwise direction, the grid inner section is at 3.5 chords from the rotor tip, i.e. at mid span of the blade. The outer spanwise grid boundary is also located 3.5 chords beyond the blade tip.

The small disturbances results are those performed by Desopper and already shown in [6]. The grid used in these computations has $70 \times 23 \times 30$ points in the ξ, η and ζ directions. The grid boundaries in the spanwise direction also are set at 0.5 R and 1.5 R for the inner and the outer boundaries respectively. In the x direction, the grid goes from about -9 chords to 6 chords from the blade and also 6 chords away from the blade in the vertical direction.

Both full potential codes use a time step equal to a quarter of degree of rotor motion. This time step is much away from the stability condition present in the FP3D code and a spanwise grid resolution twice smaller could have been run too. The time step used in the small disturbances computation is equal to 5 degrees for the nonlifting cases and to 1 degree for the lifting case.

3.2 Computed results

3.2.1 Nonlifting computations

The nonlifting computations correspond to the following conditions: advance ratio $\mu = 0.5$, rotor rotational speed $M_{\omega R} = 0.64$, blade aspect ratio

$AR = 7.$, blade airfoil NACA 0011. Three blade tip geometries were computed: a rectangular blade, a 30° aft swept tip and a 30° forward swept tip.

The results found with the FP3D code show a very good correlation with those obtained by Desopper in [6]. Qualitatively, the iso-Mach lines (figures 3 and 4) show that the same features found with the small disturbances code are found with the FP3D code when the blade tip shape is swept forward or aft: the transonic effects are reduced for the aft swept tip compared to the rectangular one in the first quadrant but the opposite effect can be observed in the second one; an opposite effect is observed for the forward swept tip. The supersonic zone found with both codes has the same shape and position. One can note, however, that the shocks appear to be slightly stronger with the small disturbances code and this may be due to the better grid resolution near the tip (at the blade tip, the spanwise distribution of the grid sections for the FP3D code was obtained by taking one section over two from the one used in the small disturbances computation; the same spanwise grid distribution was used elsewhere). The evolution of the maximum local Mach number (figures 5 and 6) shows that the results also correlate well quantitatively since about the same Mach levels can be observed. However, one can note that the effect of the blade tip sweep appears to be slightly more important on the small disturbances results. It is also possible to note that an instability appears at the blade tip, for $\psi = 150^\circ$, on the FP3D results; the biasing scheme seems not to be satisfactory enough for this severe case and it has to be improved.

The results obtained with the FPR code show more differences with the previous results analysed. The iso-Mach lines (figures 7 and 8) show that, basically, the same phenomena are found with this code, the shocks being set at about the same stations observed on the other results. However, it seems obvious that the shocks obtained with the FPR code are much stronger than those obtained with the other codes and that, more generally, higher velocities on the blade are obtained with this code. Naturally, since there is no experimental data available, it is impossible to say which results are the more plausible; one can only note that in [6] Desopper got fairly good comparisons with experiment for high speed cases with his advanced small disturbances formulation. On the other hand, the FPR code compared well with other existing Full Potential codes for less severe test cases [21], but it is the first time that very high speed cases are computed with this code.

A possible explanation of these important differences between the two full potential codes may be the lack of a consistent metrics differencing in the FPR code. This problem is under investigation since a fully consistent metrics differencing is under development on the FPR code. Another element of discussion is that it has been observed, for both full potential codes that these high speed cases are close to the stability limits of the numerical methods, and this may explain some differences. Anyway, no absolute answer can still be given to explain the differences observed and further investigations are necessary.

3.2.2 Lifting computation

The lifting computation performed with the FP3D code is a configuration

tested with a 3 bladed model rotor in the ONERA S2CH wind tunnel. The flight parameters are: $C_T/\sigma = 0.075$, $V_0 = 91\text{ m/s}$, $\omega R = 210\text{ m/s}$. A simple Drees downwash model has been used for inflow modelling, as Desopper made in his paper. The unsteady lifting computations are made on an isolated blade with an angle of attack prescribed along the blade for each azimuthal location using the experimental rotor shaft angle, collective pitch angle, blade twist angle and flapping.

The computational results (figures 9 and 10) show that the small disturbances results appear to be generally better than those obtained with the FP3D code. This is particularly obvious for the azimuthes where strong shocks can be observed ($\psi = 90^\circ$, $\psi = 120^\circ$ and $\psi = 150^\circ$); there, the supercritical zone extent found by the FP3D computation is smaller and the shock intensity weaker than those obtained by experiment and the small disturbances computation. This can probably be explained by the poor grid resolution in the spanwise direction at the blade tip which tends to increase the tip effects and therefore to reduce the velocities computed.

However the general agreement is fairly satisfactory for these first computations and after a more systematic study of the computational parameters, one can hope to be able to compute rotor flows with a sufficient accuracy to use the method in a design process.

4 Conclusion

Two finite difference rotor codes (FPR and FP3D) solving the conservative full potential equation have recently been developed; this paper has shown their ability to compute the flow on helicopter rotor blades for various blade tip shapes.

The results obtained for nonlifting cases demonstrate that both codes describe qualitatively well the influence of blade tip sweep on the transonic flow over the blade and these results correlate fairly well with those obtained by Desopper using an advanced small disturbances formulation. However, quantitatively, important differences have been observed between the FPR results and the FP3D or the small disturbances results. These differences are difficult to explain since several parameters may influence significantly the results: grid differencing, grid resolution... In particular, the lifting case computed by the FP3D code has shown that the grid refinement in the spanwise direction is insufficient at the blade tip to get a good correlation with measurements. Consequently further investigations are needed to have a better idea of the problem. Anyway, the computed cases shown above for nonlifting flow are very severe test cases with very high speed, they are probably close to the limits of the theory, and one can suppose the agreement would be better for less severe cases.

However, both full potential methods may be improved in various areas (metric differencing, switching method...), and some work is underway for that; therefore, the computations performed in this paper should be improved in accuracy and reliability in the near future.

References

- [1] Caradonna F.X. and Philippe J.J. "The flow over a helicopter blade tip in the transonic regime", *Vertica*, Vol.2,1978, pp.43-60
- [2] Philippe J.J. and Chattot J.J. "Experimental and theoretical studies on helicopter blade tips at ONERA", Sixth European Rotorcraft Forum, Sept.1980, ONERA T.P. No 1980-96
- [3] Arieli R. and Tauber M.E. "Computation of subsonic and transonic flow about lifting rotor blades", AIAA Paper 79-1667, Aug.1979
- [4] Chang I-Chung and Tung C. "Numerical solution of the full-potential equation for rotors and oblique wings using a new wake model", AIAA Paper 85-0268, Jan.1985
- [5] Johnson W. "A lifting surface solution for vortex airloads and its application to rotary wing airloads calculations", ASRL TR-153-2, Apr.1970
- [6] Desopper A. "Study of the unsteady transonic flow on rotor blades with different tip shapes", Tenth European Rotorcraft Forum, Aug.1984
- [7] Chattot J.J. and Philippe J.J. "Pressure distribution computation on a non-lifting symmetrical helicopter blade in forward flight", La Recherche Aérospatiale No 1980-5, Sept.1980
- [8] Desopper A., Caradonna F.X. and Tung C. "Finite difference modeling of rotor flows including wake effects", Eighth European Rotorcraft Forum, Sept.1982
- [9] Desopper A., Lafon P., Philippe J.J. and Prieur J. "Effect of an anhedral sweptback tip on the performance of a helicopter rotor", Thirteenth European Rotorcraft Forum, Sept.1987
- [10] Prieur J., Lafon P., Caplot M. and Desopper A. "Experimental and analytical transonic aerodynamic and acoustic results for rectangular and swept rotor blade tips", National Specialists Meeting on Aerodynamics and Acoustics, Fort Worth, Texas, Feb.1987
- [11] Desopper A., Chopra I. and Kim K. "Dynamic blade response calculations using improved aerodynamic modeling", National Specialists Meeting on Aerodynamics and Acoustics, Fort Worth, Texas, Feb.1987
- [12] Steger J.L. and Caradonna F.X. "A conservative implicit finite difference algorithm for the unsteady transonic full potential equation", AIAA Paper 80-1368, Jul.1980
- [13] Chang I-Chung "Transonic flow analysis for rotors, Part 2, Three dimensional unsteady full potential calculation", NASA Technical Paper

2375, Jan.1985

- [14] Strawn R.C. and Caradonna F.X. "Numerical modeling of rotor flows with a conservative form of the full potential equation", AIAA Paper 86-0079, Jan.1986
- [15] Strawn R.C. and Tung C. "The prediction of transonic loading on advancing helicopter rotors", Presented at the AGARD/FDP Symposium on Applications of CFD in Aeronautics, Aix-en-Provence, France, Apr.1986
- [16] Strawn R.C. and Tung C. "Prediction of unsteady transonic rotor loads with a full potential rotor code", 43rd Annual Forum of the American Helicopter Society, St.Louis, MO, May 1987
- [17] Bridgeman J.O., Steger J.L. and Caradonna F.X. "A conservative finite difference algorithm for the unsteady transonic potential equation in generalized coordinates", AIAA Paper 82-1388, Aug.1982
- [18] Jones H.E. "Full potential modeling of blade-vortex interactions", Ph.D. thesis, George Washington University, Feb.1987
- [19] Jones H.E. and Caradonna F.X. "Full potential modeling of blade-vortex interactions", Twelfth European Rotorcraft Forum, Sept.1986
- [20] Bredif M. "Finite element calculation of potential flow around wings", 9th ICNMF, Jun.1984
- [21] Caradonna F.X. and Tung C. "A review of current finite difference rotor flow methods", 42nd Annual Forum of the American Helicopter Society, Washington D.C., Jun.1986

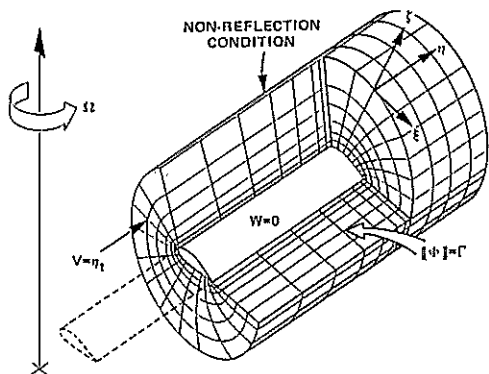


Fig.1: FPR code - Grid and boundary conditions for a rotor computation

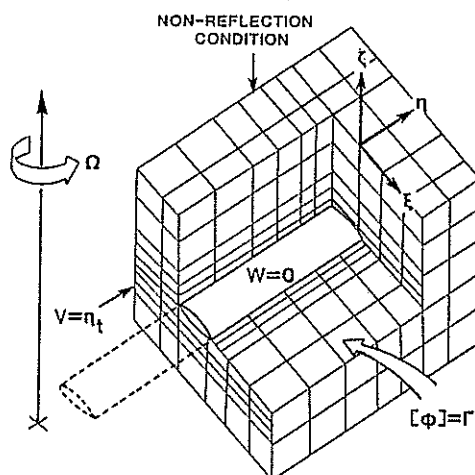


Fig.2: FP3D code - Grid and boundary conditions for a rotor computation

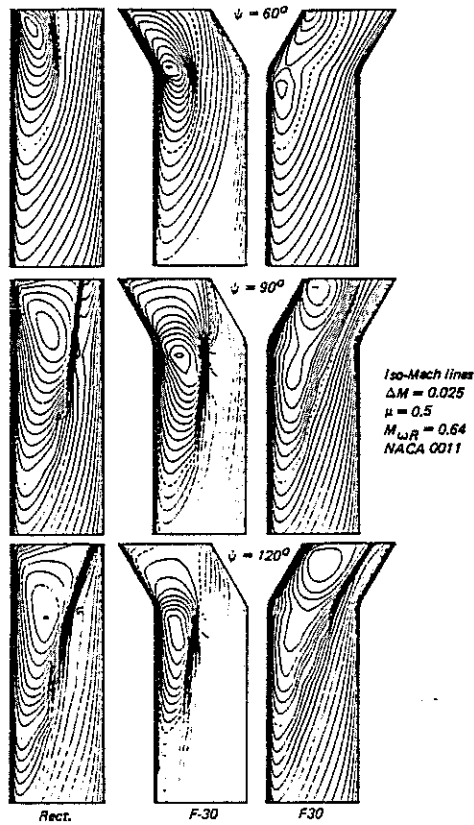


Fig.3: Study of different tip shapes - Small Disturbances
nonlifting unsteady calculations

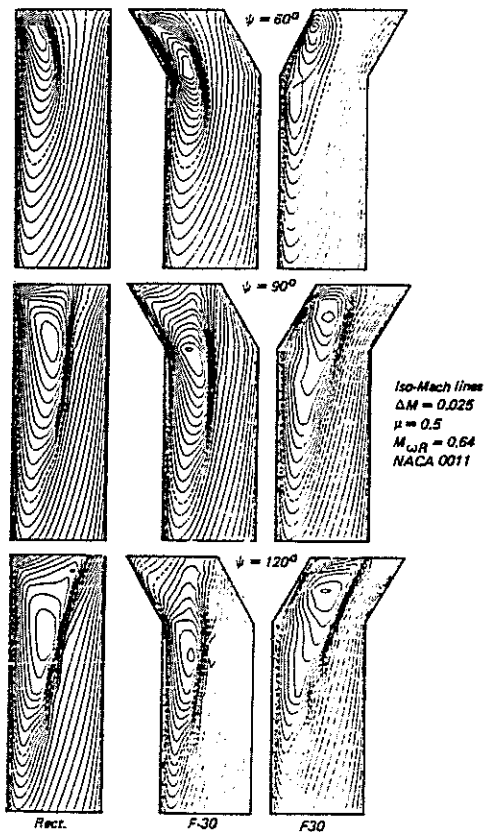


Fig.4: Study of different tip shapes - FP3D
nonlifting unsteady calculations

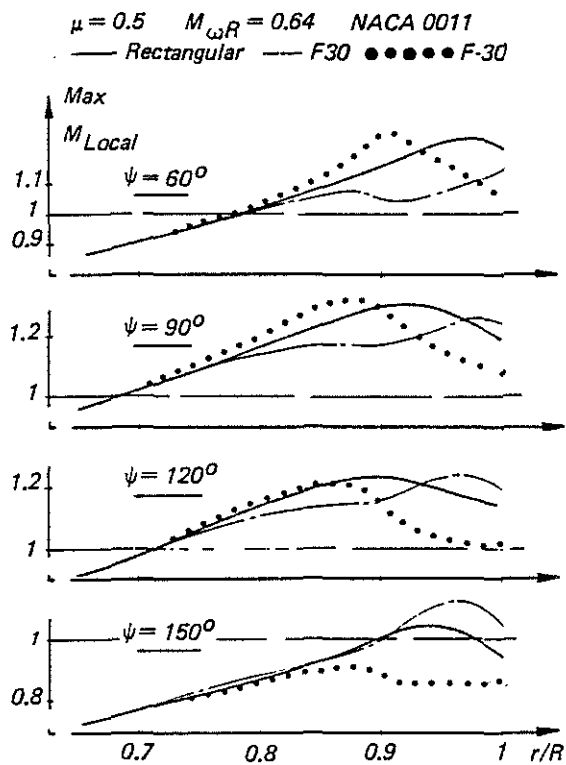


Fig.5: Study of different tip shapes
 Small Disturbances nonlifting unsteady
 calculations

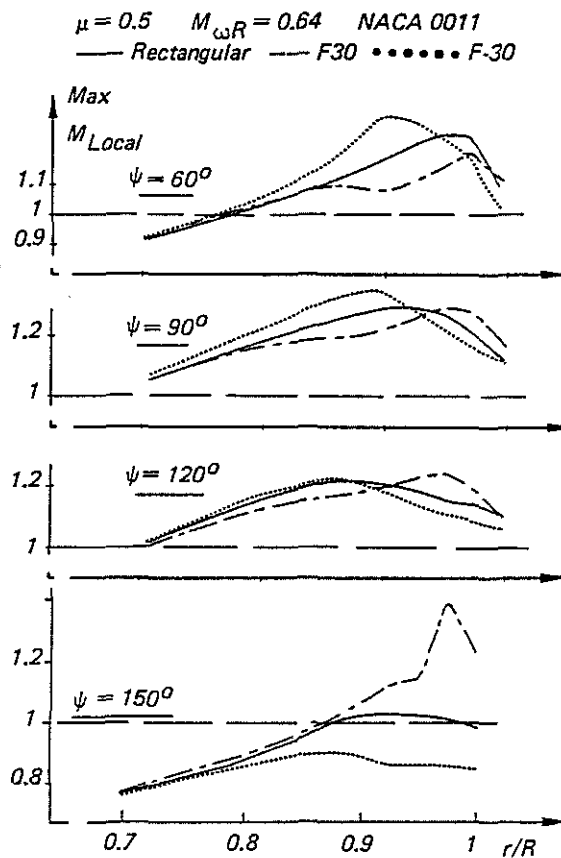


Fig.6: Study of different tip shapes
 FP3D nonlifting unsteady calculations

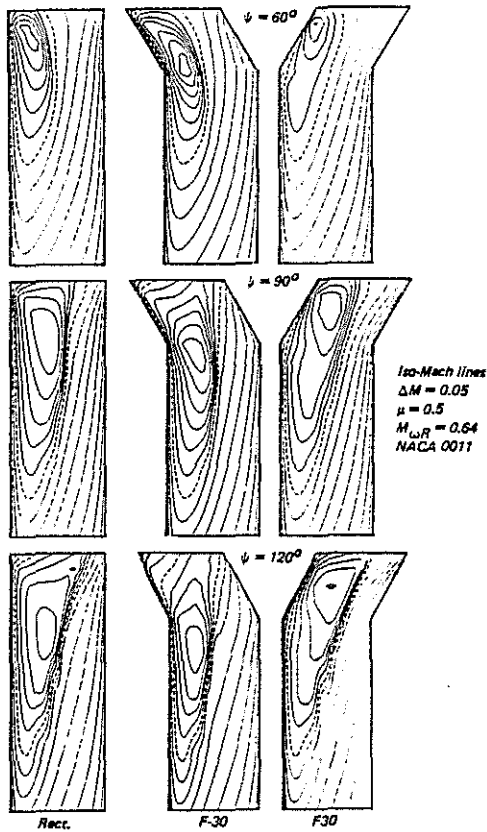


Fig.7: Study of different tip shapes - FP3D nonlifting unsteady calculations

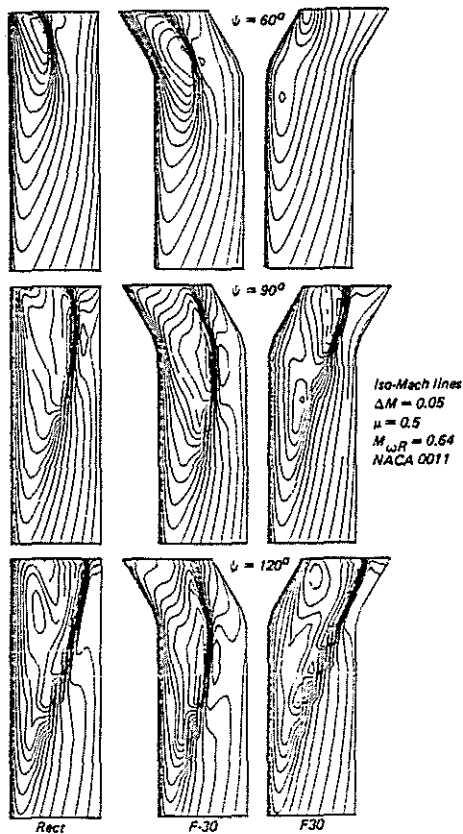


Fig.8: Study of different tip shapes - FPR nonlifting unsteady calculations

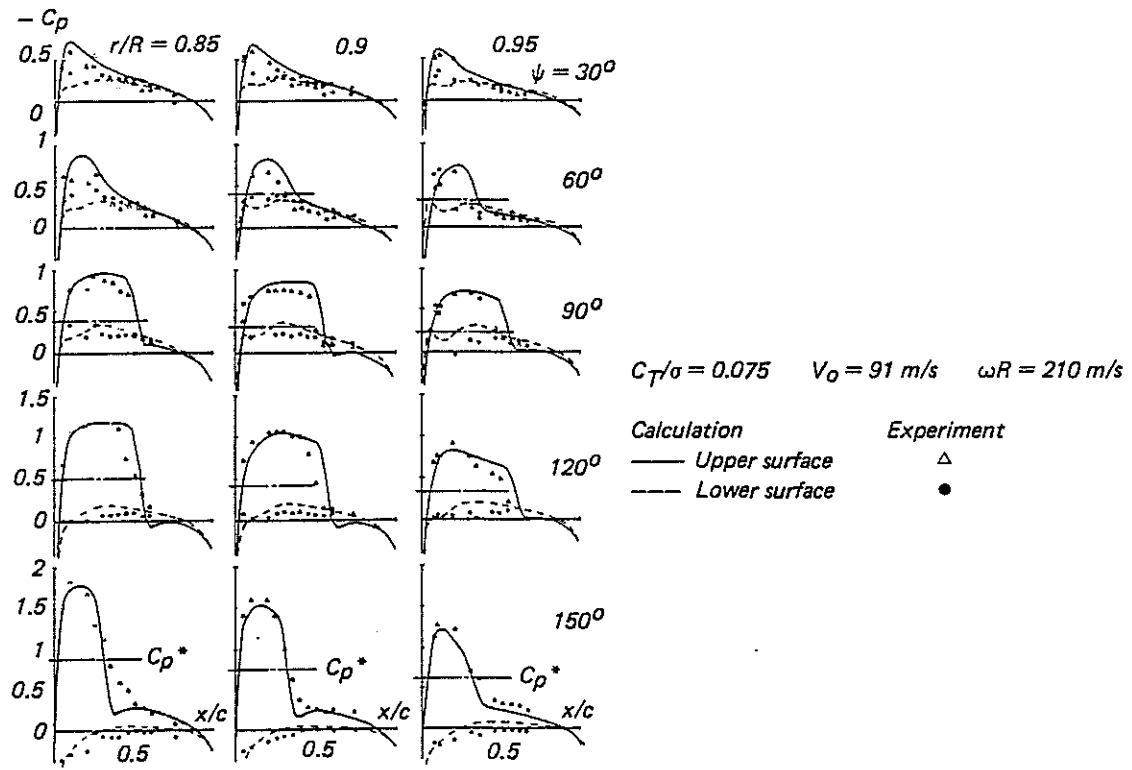


Fig.9: Small Disturbances lifting unsteady calculation - Rectangular blade

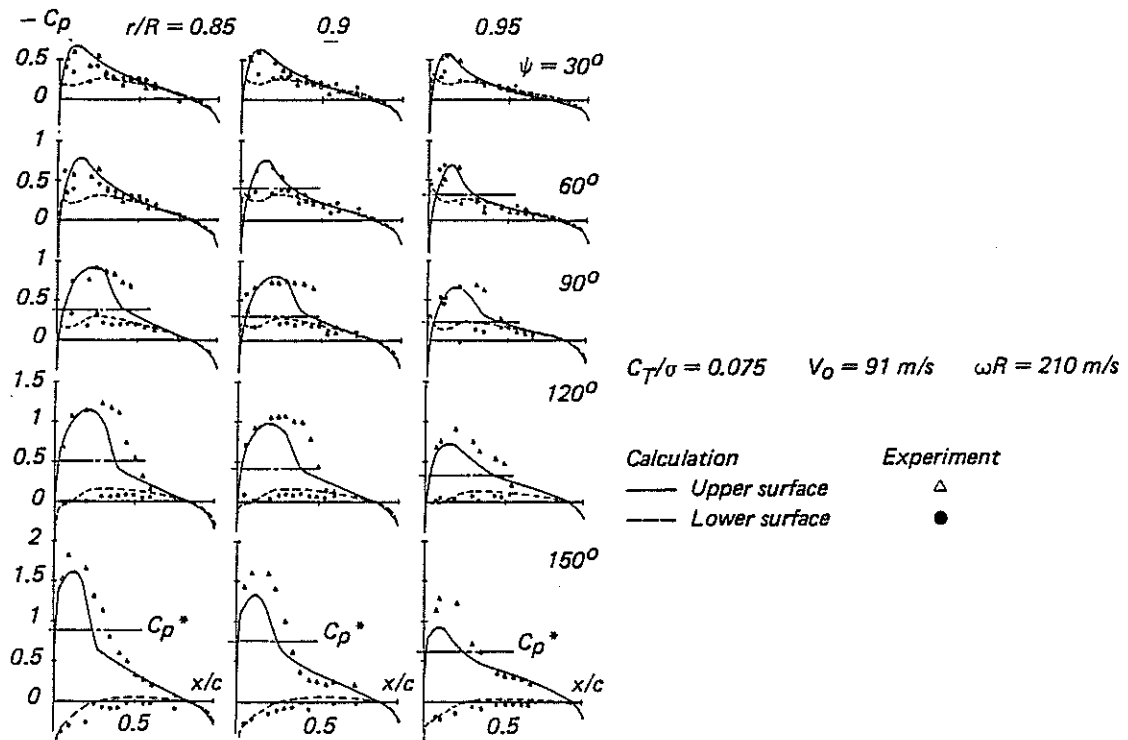


Fig.10: FP3D lifting unsteady calculation - Rectangular blade